Crystal Structure Solution of Radiation-Sensitive Porous Framework CL30 by Low-Dose Cryo 3D Electron Diffraction

Ke Wang(王科)[1,2], Dapeng Sun(孙大鹏)[2], Penghe Li(李鹏贺)[2], Zhiyuan Mao(毛志远)[2], Yi Luo(罗翼)[4], Hongxia Wang(王红霞)[1*], Hongyi Xu(徐弘毅)[3*], and Yumei Wang(王玉梅)[2*]

[1]*College of Materials Science and Engineering, Shanxi Key Laboratory of Advanced Magnesium-Based Materials, Taiyuan University of Technology, Taiyuan 030024, China*
[2]*Beijing National Laboratory for Condensed Matter Physics, Institute of Physics, Chinese Academy of Sciences, Beijing 100190, China*
[3]*Research School of Chemistry, Australian National University, Acton ACT 2601, Australia*
[4]*State Key Laboratory of Green Chemical Engineering and Industrial Catalysis, Sinopec Shanghai Research Institute of Petrochemical Technology, Shanghai 201208, China*

(Received 24 December 2025; accepted manuscript online 10 February 2026)

To overcome the limitations of traditional single-crystal X-ray diffraction (SCXRD) for microcrystalline materials and the peak-overlapping issue of powder X-ray diffraction (PXRD), this study employed cryogenic continuous rotation electron diffraction (cryo-cRED) with a low-dose strategy to determine the crystal structure of CL30, a novel silicogermanate framework. It is confirmed that CL30 crystallizes in the $C2/m$ space group and has layered topology composed of discontinuous zigzag chains connected by double four-membered ring (d4r) units, with fluoride anions (F^-) occluded in the d4r units. In CL30, charge balance involves organic structure-directing agent (OSDA) cations, occluded F^-, and terminal oxygen sites whose protonation state cannot be established from the present three dimensional (3D) ED data. F^- encapsulated in the d4r units contributes to charge compensation as the counter-anion to OSDA cations, rather than only balancing the framework charge. Although the refinement indices ($R_1 = 0.29$, $wR_2 = 0.71$) exceeded typical small-molecule crystallography standards, the structural model remained highly reliable, as supported by geometric restraints and validation. In electron diffraction, elevated R_1 values are commonly attributed to the intrinsic factors of the technique, such as dynamic scattering, detector noise from scintillator-based detectors, and TEM stage instability (large spheres of confusion). This study introduces a new structural prototype to the silicogermanate family and establishes a feasible workflow for determining the structures of radiation-sensitive microcrystalline porous materials.

DOI: 10.1088/0256-307X/43/3/030717 CSTR: 32039.14.0256-307X.43.3.030717

1. Introduction. Zeolites[1] are crystalline porous materials constructed from corner-sharing TO_4 tetrahedra (T = Si, Al, B, P, Ge, Ga, etc.).[2] Owing to their molecular-scale channels, tunable compositions, and diverse morphologies, they exhibit excellent performance in catalysis, gas adsorption/separation, and ion-exchange applications. These macroscopic properties are inherently determined by their microscopic structural features, especially the pore size and channel dimensionality.[3–6] Prior to the development of three-dimensional electron diffraction (3D ED)[7,8] technology, conventional single-crystal X-ray diffraction (SCXRD) is the primary method for obtaining atomic-level structural information, but it required high-quality single crystals typically larger than $5 \times 5 \times 5\,\mu m^3$.[9] However, most zeolites, especially one-dimensional or two-dimensional systems, can only be synthesized as nano- to submicron-sized crystals owing to kinetic and thermodynamic constraints.[10] The inability to grow large single crystals has limited large-scale synthetic screening and structural characterization of such materials. Although powder X-ray diffraction (PXRD) is widely used for polycrystalline structural analysis, peak overlapping often reduces the accuracy of peak assignment and intensity measurements.[11,12] The difficulty of obtaining structural solutions is further intensified for materials with large unit cells or multiphase compositions.[9,13]

When exposed to high-energy electron beams (hundreds of kilovolts) in transmission electron microscopy (TEM), beam-sensitive zeolites are prone to multiple types of radiation damage[14] including knock-on displacement, radiolysis, electrostatic charging, and heating.[14,15] These processes cause irreversible damage, including phase separation, phase transition, amorphization, mass loss, precipitation, and valence reduction.[16] Such damage severely restricts the application of electronic crystallographic techniques. However, cryogenic low-dose strategies have proven to be effective in mitigating such damage and improving data quality.[17,18]

3D ED technology offers distinct advantages for analyzing beam-sensitive crystals owing to its short wavelength and strong interaction with the matter of electrons. The higher scattering cross-section of electrons enables

*Corresponding authors. Email: wanghxia1217@163.com; hongyi.xu1@anu.edu.au; wangym@iphy.ac.cn
© 2026 Chinese Physical Society and IOP Publishing Ltd. All rights, including for text and data mining, AI training, and similar technologies, are reserved.

diffraction data collection from nanocrystals smaller than 200 nm,[19] thereby overcoming the "microcrystal limitation" of conventional SCXRD.[20] Unlike X-rays, which scatter from the total electron density of the crystal, electron diffraction is dominated by the interaction of incident electrons with the crystal's electrostatic potential,[21] making 3D ED more sensitive to light elements such as H and Li, as well as being advantageous for characterizing hydrated or hydroxyl-bearing materials.[13,22] Furthermore, cryogenic low-dose data-collection strategies have been shown to effectively reduce beam damage.[17] For instance, Sun *et al.* successfully resolved the structures of several radiation-sensitive covalent organic frameworks (COFs)[23] using cryogenic continuous rotation electron diffraction (cryo-cRED).

CL30 is a novel two-dimensional layered silicogermanate that can only be synthesized as nano- to submicron-sized crystals whose atomic structure cannot be resolved by conventional SCXRD. Moreover, the radiation-sensitivity of CL30 severely restricts its application to traditional electron microscopy techniques. Although low-dose cryogenic 3D ED has been demonstrated for zeolites/silicates and related porous frameworks, reliable structural solutions for CL30 remain challenging owing to their combined radiation sensitivity and weak diffraction. Therefore, reliable structural determination is essential not only to understand the intrinsic features of its layered framework, but also to evaluate its potential as a precursor for 3D porous materials. In this study, we report the first structural determination of CL30 using cryo-cRED[8,24] with 200 kV Glacios TEM. By tilting the specimen stage, multiple 3D cRED datasets were acquired within minutes and merged to achieve a data completeness of 76.5%. Under liquid-nitrogen temperature and ultra-low electron dose conditions, the layered framework of CL30 was successfully resolved, thus establishing a new layered silicogermanate structural prototype and developing a practical cryo-cRED workflow for radiation-sensitive microcrystalline silicogermanates. This study aimed to clarify the crystal structure characteristics of CL30, verify the applicability of cryo-cRED for characterizing radiation-sensitive microcrystalline silicogermanates, and provide a technical reference for the structure determination of similar materials.

2. Experimental.

2.1. Synthesis of CL30 Zeolite. The reaction gel was prepared with a molar composition of 0.6 SiO_2 : 0.4 GeO_2 : 0.5 OSDAOH : 2 HF : 3 H_2O. Typically, 0.6 mmol of fumed silica and 0.4 mmol of GeO_2 were gradually added to 10 mL of the OSDAOH solution, followed by magnetic stirring for 30 minutes until complete dissolution. After the dropwise addition of HF (2 mmol), stirring was continued for 1 h to form a homogeneous gel. The gel was transferred into a 23-mL Teflon-lined autoclave and crystallized at 383 K for 7 days. The solid product was collected by centrifugation, washed repeatedly with deionized water, and dried overnight at 353 K to obtain the CL30 powder samples.

The crystallinity of CL30 was evaluated using PXRD. Samples with clear diffraction peaks and narrow full-widths at half-maximum (FWHM) in the $2\theta > 40^\circ$ range ($d < 2.25$ Å)[25] were selected for subsequent analysis. Note that peak broadening due to size effects can become significant when crystal dimensions approach tens of nanometers.[26] Therefore, crystallinity was evaluated based on the peak position, intensity, and number rather than the peak width alone.[18] CL30 exhibited multiple distinct high-angle diffraction peaks, indicating good crystallinity and suitability for 3D ED investigations.

2.2. TEM Sample Preparation. Specimens for TEM observations were prepared by dispersing the powder in anhydrous ethanol, gently grinding it in an agate mortar, and ultrasonically treating it in a water bath for approximately 30 minutes. This was performed to ensure that the single crystals located over the holes in the TEM grid were as thin as possible (typically < 200 nm).[27] The resulting suspension was dropped onto a carbon-supported copper grid and dried at room temperature. The grid was then clipped using C-O rings under liquid-nitrogen conditions. The 3D ED data were collected using a 200 kV cryo-TEM (Thermo Fisher Glacios, equipped with a Schottky XFEG field-emission gun and a Ceta CMOS camera).

2.3. 3D ED Data Acquisition.

2.3.1. cryo-cRED Data Collection. 3D ED data were collected using a Thermo Fisher Glacios 200 kV cryo-TEM (Schottky X-FEG field-emission gun, equipped with a Ceta CMOS camera) at the liquid-nitrogen temperature (77 K). To minimize beam damage, all acquisitions were performed in the low-dose mode within SerialEM.[28] First, the grid was rapidly screened at low magnification (3400×) to locate suitable crystals, which were then recorded. After switching to near-parallel illumination, a target CL30 crystal was selected at a 0° tilt, and a feature on the nearby carbon film was selected as the mechanical eucentric reference. The stage was tilted to +20°, and the Z height was adjusted to recenter the reference, thereby setting the eucentric height. This alignment was verified by tilting to −20° to minimize lateral displacement, as shown in Fig. 1.[18]

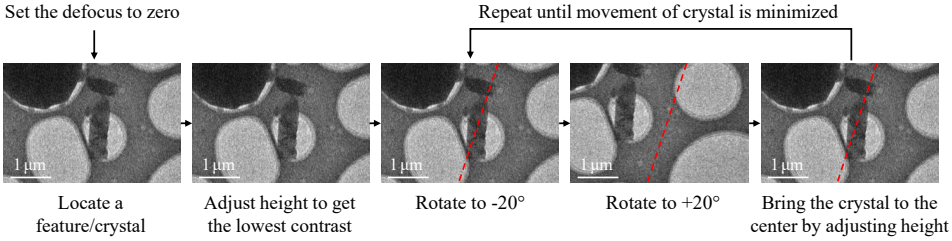

Fig. 1. Illustration of eucentric height adjustment.

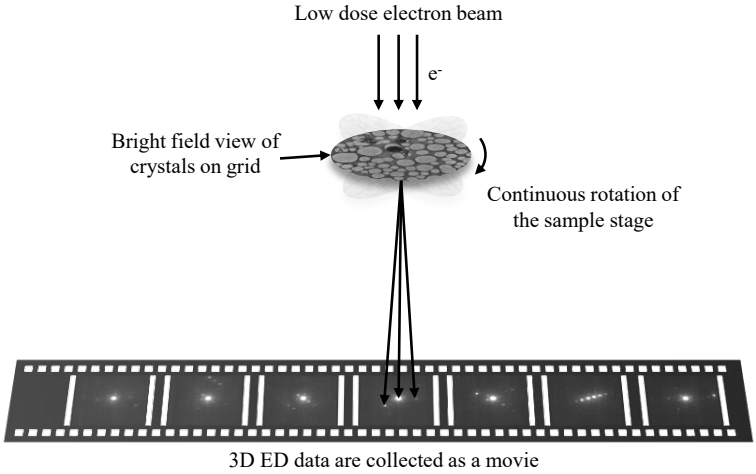

Fig. 2. Workflow for continuous-rotation 3D electron diffraction data collection.

After eucentric alignment, cRED data collection was initiated by rotating the goniometer to a predetermined start angle, inserting an appropriately sized selected-area aperture to define the illuminated region, switching to diffraction mode, and recording in movie mode, as shown in Fig. 2.

Data were collected at 200 kV with a spot size of 10 and camera length of 850 mm. A continuous rotation range of $-55°$ to $+55°$ was covered in steps of $0.27°$, with each frame exposed for 0.2 s. The flux density was $0.21\,e^{-}\cdot Å^{-2}\cdot s^{-1}$, resulting in a per-frame fluence of $0.042\,e^{-}\cdot Å^{-2}$, and a total accumulated fluence of $17.3\,e^{-}\cdot Å^{-2}$. No beam stop was used to preserve low-angle diffraction information. To improve the data completeness, several cRED datasets were collected from multiple well-oriented crystals on the same grid and merged during structural solution and refinement. Under these cryogenic low-dose parameters, high-quality 3D ED data with a sufficient signal-to-noise ratio and resolution were obtained, providing a reliable basis for subsequent structure determination.

2.3.2. 3D ED Data Processing. The instrument was calibrated prior to data processing. The ROTATION_AXIS was manually determined to be $-92.9°$ via goniometer tilt experiments on a standard crystal.[29] Using the known zeolite SCM-15 as a reference, the 3D reciprocal space was reconstructed in REDp, and unit cell parameters were refined to calibrate the reciprocal space pixel size (CCDPIXELSIZE = $0.002780\,Å^{-1}$) at a camera length of 850 mm.

Subsequently, the collected cRED data were processed to batch convert TIFF image sequences to MRC format and extract tilt angles for the REDp input file (.ed3d) using IMOD with custom scripts (read_angle.sh and convert_mrc.sh). The file was configured with the following parameters: WAVELENGTH = 0.02508 Å (200 kV), ROTATION_AXIS = $-92.9°$, CCDPIXELSIZE = $0.002780\,Å^{-1}$, GONIOTILTSTEP = $0.27°$, and OSCILLATION_RANGE = (end angle – start angle)/(number of frames -1).

For the CL30 cRED data, drift correction (using the transmitted-beam spot in the first frame as a reference), peak searching, and 3D reciprocal space reconstruction were sequentially performed in REDp. Automatic unit cell determination was unstable owing to noise, streaks, and some elongated diffraction spots. Consequently, the directions and lengths of a^*, b^*, and c^* were manually defined, reflections with obvious noise were removed, and the systematic absences observed from the reconstructed 3D reciprocal lattice shown in Figs. 3(a)–3(d) were initially consistent with an I-centered monoclinic structure ($I2$, Im, or $I2/m$). This lattice was reindexed to a conventional C-centered monoclinic setting (unique axis b) for subsequent XDS/XSCALE processing, yielding space group candidates $C2$, Cm, or $C2/m$, consistent with the 3D reflection distribution and systematic extinction features. The indexing solution (unit cell and orientation) obtained from the 3D reciprocal space reconstruction in REDp was used to generate the XDS input files.

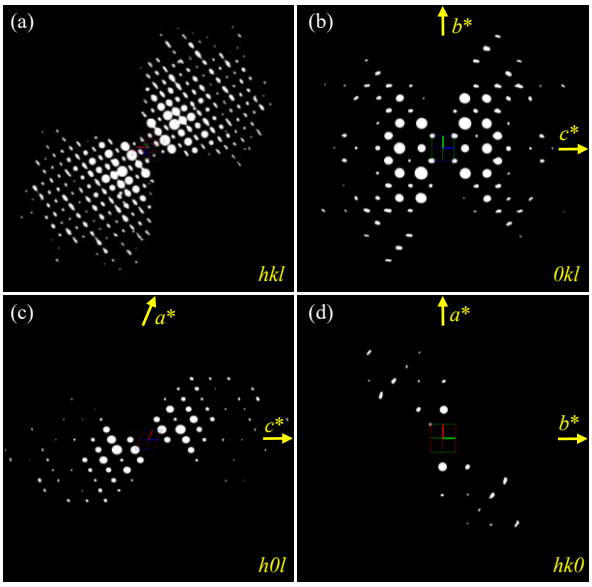

Fig. 3. (a) Reconstructed three-dimensional reciprocal lattice of CL30 based on SCED data. Derived from the 3D lattice and 2D slices (b) $0kl$, (c) $h0l$, (d) $hk0$, the reflection conditions are deduced as: hkl: $h+k+l=2n$, $h0l$: $h+l=2n$, $0k0$: $k=2n$. The possible space groups are $I2$, Im, or $I2/m$; the corresponding standard settings are $C2$, Cm, or $C2/m$, respectively.

Raw diffraction frames were then processed using XDS for indexing refinement, intensity integration, and scaling (merged with XSCALE when applicable), followed by structural solution and refinement in SHELXT/SHELXL.

Following cryo-cRED data acquisition and preprocessing in the REDp, a representative single-crystal electron diffraction (SCED) dataset was processed using XDS. The dataset was reliably indexed to a C-centered monoclinic system with unit cell parameters $a = 18.19$ Å, $b = 15.18$ Å, and $c = 13.61$ Å, $\beta = 112.56°$, consistent with the reconstructed 3D reciprocal lattice. The data completeness was approximately 65.2%, with the highest resolution approaching 1.0 Å. XPREP was used to assess the systematic absences and intensity statistics of the integrated data to identify plausible space group candidates. The trial structure solutions in SHELXT showed that only $C2/m$ yielded a chemically and topologically reasonable framework model and was therefore adopted as the final space group.

3. Results and Discussion.

3.1. Structure Solution and Refinement. In the $C2/m$ space group, the CL30 structure was directly solved from cryo-cRED data intensity using SHELXT. The solution revealed six symmetrically independent T-sites (Si/Ge) and fifteen symmetrically independent oxygen sites, consistent with a layered framework in which the zigzag chains are terminated by terminal oxygen atoms. The initial model was refined in SHELXL;[30] however, due to streaks caused by the thin-plate morphology and missing diffraction information along the c-axis, anisotropic refinement could not be performed. To ensure chemical and geometrical reasonableness while reducing the number of refined parameters, RIGU/SIMU restraints on the atomic displacement parameters and DFIX/SADI distance restraints on the T-O bonds were applied. These restrains the T-O bond lengths to a reasonable range and improves the geometric and chemical consistency of the model.

The layered topology of CL30 is shown in Fig. 4. Each layer consists of interrupted zigzag chains connected to double four-ring (d4r) units, as shown in Fig. 4(b). These layers are stacked in a simple AAAA sequence, as shown in Figs. 4(c) and 4(d). The zigzag chains are terminated by oxygen atoms, creating an interlayer spacing of approximately 3.2 Å between adjacent terminal O atoms. The intralayer distances were approximately 9.1 Å, 8.5 Å, and 6.6 Å, respectively. Within this layer, the eight-membered ring micropores are surrounded by two zigzag chains and two d4r units.

Owing to the limitations in the intensity and accuracy of the 3D ED data, the Si/Ge occupancies at the individual T-sites were not refined. Instead, all T-sites were modeled as Si, with the overall Si/Ge ratio fixed at 0.6 SiO_2 : 0.4 GeO_2 based on the synthesis gel composition and bulk elemental analysis. According to previous reports,[31] Ge preferentially occupies d4r sites. Consequently, Ge enrichment in the d4r units can be qualitatively proposed without quantitative modelling.

An unrestrained difference Fourier map ($F_o - F_c$) of the electrostatic potential revealed a stable residual peak inside the d4r cage, consistent with an F^-. Due to F^- located at the center of the cage is lighter without directional covalent bonds, and the limited intensity and parameter ratio of the 3D ED data in this study, this F^- site was refined isotropically without any geometric constraints on the F-T distance. The refinement indicated that each d4r unit contains approximately one F^-, with F-T bond lengths falling within the reported range for silicogermanate d4r units.[31] This result further confirms that during synthesis, the incorporated HF in the reaction gel provides F^-. In fluoride-mediated synthesis, F^- is commonly incorporated into d4r cages to charge-balance OSDA cations; in silicogermanate zeolites, Ge typically preferentially occupies T sites in d4r units.[32] The structural model of F^- in the d4r units is shown in Fig. 5.

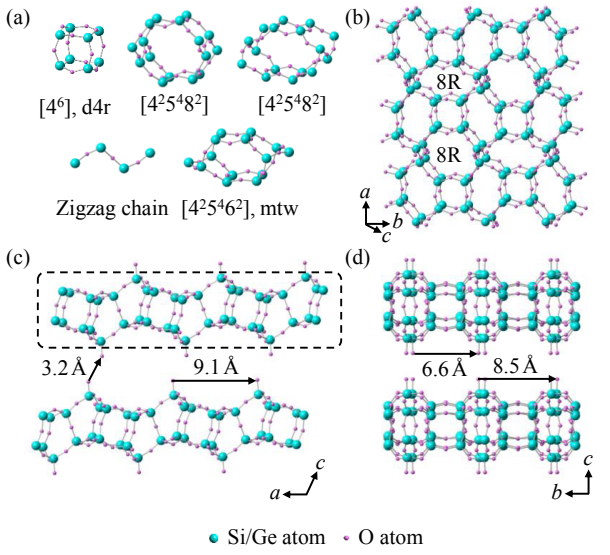

Fig. 4. Layered framework structure of CL30. (a) The composite building units in CL30; (b) the layered framework topology; projections viewed along the (c) b-axis and (d) a-axis. F are omitted for clarity.

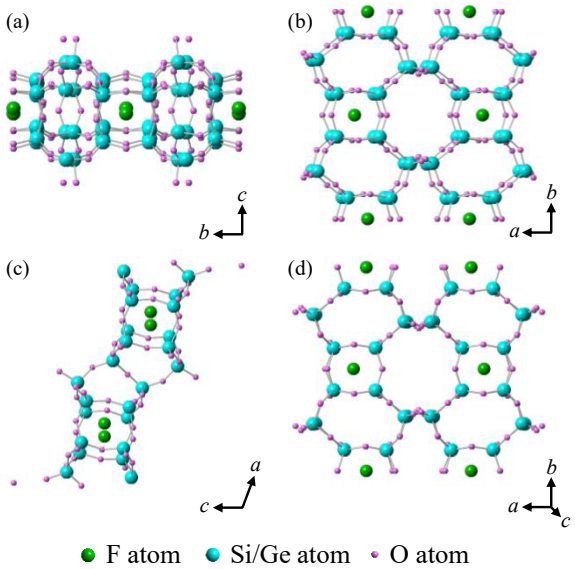

Fig. 5. Structural model showing the location of F^- at the centers of the d4r cages in CL30. Panels (a)–(d) show projections along different crystallographic directions.

Table 1. Crystallographic Data and Structure Refinement Results for CL30.

Method	cRED
No. of data sets merged	7
Wavelength (Å)	0.02508
Resolution (Å)	1.0
Empirical formula	$FO_{25}Si_{12}$[a]
Crystal system	Monoclinic
Space group	$C2/m$
Unit cell a, b, c (Å)	18.19(4), 15.18(3), 13.61(3)
β (°)	112.56(3)
No. of unique reflection ($F > 4\sigma(F)$/all)	757/1471
Completeness	76.5
$CC_{1/2}$	99.6
No. of parameters	82
No. of restraints	9
$R_1[F > 4\sigma(F)/R_1(\text{all})]$	0.2864/0.3626
R_{int}	0.4974
GOF	1.058

[a]Note: The formula in Table 1 reflects the refined inorganic model (framework + occluded F^-); OSDA and H at terminal O sites are not included due to insufficient observability in the present 3D ED data.

Due to limited data resolution and signal-to-noise ratio, no clear OSDA (diisopropylethylmethylammonium) signals were observed in the difference electrostatic potential map ($F_o - F_c$). Therefore, only the framework and d4r F^- inside the d4r units were revealed in the final structural model. The refinement converged to $R_1 = 0.29$ [$I > 4\sigma(I)$], $R_1 = 0.36$ (all data), and $wR_2 = 0.71$. The crystallographic data and refinement parameters of CL30 are listed in Table 1.

3.2. Structure Validation. Although the structure validation triggered several A-level alerts, including $R_{\text{int}} = 0.4974$, $\sin(\theta_{\max})/\lambda = 0.500$, reflection completeness of 76.5%, $R_1 = 0.29$, $wR_2 = 0.71$, and a solvent-accessible void warning, these deviations are reasonable for a weakly diffracting, highly porous Si/Ge framework obtained from limited-quality data. Systematic examination of the model's geometry, bond lengths/angles, thermal displacement parameters, and residual peaks in the difference electrostatic potential map ($F_o - F_c$) confirmed the self-consistency and reliability of the main framework. Therefore, this structure is suitable for subsequent analyses.

This structural model describes the primary framework of the CL30. Local disorder or stacking faults can also occur. The quality of the available 3D ED data is insufficient for the detailed modeling of disordered regions or guest molecules. An F^- site within the double d4r unit was identified based on the difference electrostatic potential map ($F_o - F_c$) and chemical consistency. The following B-level alerts were noted: elevated U_{eq} values at specific atoms likely reflected local disorder or enhanced thermal motion that could not be modeled further. These alerts mislead the F-O distances as the Inter HL...A Contacts. The reported F-O distances were normal for the d4r units and the occluded F atoms. The missing reflections persisted even after merging, which improved completeness to 76.5%. This persistence can be attributed to the inherent limitations of electron diffraction, such as dynamic scattering, detector noise from scintillator-based detectors, and TEM stage instability (a large sphere of confusion). Systematic checks of geometry, bond lengths and angles, displacement parameters, and residual peaks in the difference electrostatic potential map ($F_o - F_c$) confirmed its self-consistency and reliability under the current data constraints. Accordingly, the refined framework structure was considered reliable.

4. Conclusions. In this study, the crystal structure of the radiation-sensitive porous framework CL30 was successfully resolved using cryogenic low-dose 3D ED. We demonstrated the applicability of cryo-cRED for characterizing nanoscale, radiation-sensitive silicogermanate materials and established a data-processing workflow for similar microcrystalline-sensitive systems. The layered topology of CL30, the presence of F^- in double d4r units, and the distribution characteristics of Si/Ge were clarified for the first time. Despite inherent data limitations, rational geometric constraints and systematic structural validation were used to construct a chemically and topologically reasonable framework model, providing a basis for subsequent investigations.

Precise localization of the OSDA and quantitative analysis of the Si/Ge distribution were not achieved in this study. This is a common challenge in characterizing such porous microcrystalline materials, owing to the weak diffraction and signal limitations of 3D ED. Nevertheless, the resolved CL30 framework offers new insights into the design and functional exploration of silicogermanate materials, and provides a feasible pathway for determining the structures of radiation-sensitive microcrystalline porous materials.

Acknowledgements. This work was supported by the National Natural Science Foundation of China (Grant No. 12374021) and Beijing Natural Science Foundation (Grant No. 1252031). We thank the Beijing National Laboratory for Condensed Matter Physics, Institute of Physics, Chinese Academy of Sciences and Beijing Branch of Songshan Lake Laboratory for Materials Science for our cryo-EM work. Hongyi Xu thanks the Australian Research Council for the future fellowship.

References

[1] Dusselier M and Davis M E 2018 *Chem. Rev.* **118** 5265
[2] Luo Y, Smeets S, Wang Z D, Sun J L, and Yang W M 2019 *Chem. Eur. J.* **25** 2184
[3] Tosheva L and Valtchev V P 2005 *Chem. Mater.* **17** 2494
[4] Davis M E 2002 *Nature.* **417** 813
[5] Davis M E 2014 *Chem. Mater.* **26** 239
[6] Vermeiren W and Gilson J P 2009 *Top. Catal.* **52** 1131
[7] Kolb U, Gorelik T, Kübel C, Otten M T, and Hubert D 2007 *Ultramicroscopy* **107** 507
[8] Zhang D L, Oleynikov P, Hovmöller S, and Zou X D 2010 *Z. Kristallogr.* **225** 94
[9] Huang Z H, Willhammar T, and Zou X D 2021 *Chem. Sci.* **12** 1206
[10] Asgar Pour Z, Alassmy Y A, and Sebakhy K O 2023 *Crystals* **13** 959
[11] Wan W, Su J, Zou X D, and Willhammar T 2018 *Inorg. Chem. Front.* **5** 2836

[12] Li P S, Cui W R, Li R, Sun H L, Li Y C, Yang D L, Gong Y, Li H, and Li X D 2017 *Chin. Phys. Lett.* **34** 076201
[13] Gemmi M, Mugnaioli E, Gorelik T E, Kolb U, Palatinus L, Boullay P, Hovmöller S, and Abrahams J P 2019 *ACS Cent. Sci.* **5** 1315
[14] Egerton R F 2013 *Ultramicroscopy* **127** 100
[15] Consolaro V G, Rouchon V, and Ersen O 2024 *Microporous Mesoporous Mater.* **364** 112835
[16] Chen Q L, Dwyer C, Sheng G, Zhu C Z, Li X N, Zheng C L, and Zhu Y H 2020 *Adv. Mater.* **32** 1907619
[17] Bwanika H C, Zhao J J, Hofer G, Sauer U H, and Xu H Y 2025 *Acta Crystallogr. D Struct. Biol.* **81** 693
[18] Yang T M, Willhammar T, Xu H Y, Zou X D, and Huang Z H 2022 *Nat. Protoc.* **17** 2389
[19] Saha A, Nia S S, and Rodriguez J A 2022 *Chem. Rev.* **122** 13883
[20] Wu D S, Mi Z Y, Li Y J, Wu W, Li P L, Song Y T, Liu G T, Li G, and Luo J L 2019 *Chin. Phys. Lett.* **36** 077102
[21] Mu X L, Gillman C, Nguyen C, and Gonen T 2021 *Annu. Rev. Biochem.* **90** 431
[22] Yang Y P, Lin X J, Xian H Y, Chen S D, Yuan Y H, Xi J X, Zhu J X, and He H P 2024 *Acta Mineralogica Sin.* **44** 655 (in Chinese)
[23] Li J, Lin C, Ma T Q, and Sun J L 2022 *Nat. Commun.* **13** 4016
[24] Lu P, Xu J Y, Sun Y Q, Guillet-Nicolas R, Willhammar T, Fahda M, Dib E, Wang B, Qin Z X, Xu H Y, Cho J, Liu Z P, Yu H J, Yang X B, Lang Q L, Mintova S, Zou X D, and Valtchev V 2024 *Nature* **636** 368
[25] Ali A, Chiang Y W, and Santos R M 2022 *Minerals.* **12** 205
[26] Holder C F and Schaak R E 2019 *ACS Nano.* **13** 7359
[27] Nannenga B L and Gonen T 2018 *Emerg. Top. Life Sci.* **2** 1
[28] de la Cruz M J, Martynowycz M W, Hattne J, and Gonen T 2019 *Ultramicroscopy* **201** 77
[29] Wan W, Sun J L, Su J, Hovmöller S, and Zou X D 2013 *J. Appl. Crystallogr.* **46** 1863
[30] Hübschle C B, Sheldrick G M, and Dittrich B 2011 *J. Appl. Crystallogr.* **44** 1281
[31] Fischer M, Bornes C, Mafra L, and Rocha J 2022 *Chem. Eur. J.* **28** e202104298
[32] Fischer M and Freymann L 2021 *ChemPhysChem.* **22** 40